Investigation DSC and XRD on the Crystallization Kinetics in the Phosphate Li2O–Li2WO4–TiO2–P2O5 Glassy Ionic System

Hicham ES-SOUFI
Equipe de Physico-Chimie de la Matiére Condensée, PCMC, Faculté des Sciences de Meknès, Universite Moulay Ismail, Morocco https://orcid.org/0000-0002-2075-1376

L. Bih
Chimie de la Matière Condensée de Paris: Laboratoire de Chimie de la Matiere Condensee de Paris

Alan R. F. Lima (alan.quimicafct@gmail.com)
Cegep de Chicoutimi Sciences de la Nature Rod. Lauri Simoes, de Barros Km 12, 18290-000 Bauri, SP, Brazil

A. El Bouari
Laboratory of Physico-Chemical of Applied Materials, Faculty of Sciences Ben M'Sik, Hassan II University, Casablanca, Morocco

B. Manoun
Laboratoire des Sciences des Matériaux et de la Modélisation des Milieux (LS3M), Université Hassan 1er, 26000, Khouribga, Morocco

S. Hussain
School of Materials and Enginnering, Jiangsu University, Zhenjiang, 212013, China

Research Article

Keywords: Phosphate Glasses, Chemical durability, Crystallization Kinetic, Avrami parameter

Posted Date: February 15th, 2021

DOI: https://doi.org/10.21203/rs.3.rs-190511/v1

Abstract

This work aims to investigate the prepared glasses within the 20Li2O−(50−x)Li2WO4−xTiO2−30P2O5 system, with 0≤x≤15 mol%. The bonds constituting the framework of these glasses were studied by Raman spectroscopy. The data analysis of the chemical durability showed that the dissolution rates depend on the composition of each glass. Thermal analysis by DSC technique was used to determine the activation energy of crystallization, it found in the glass of composition (x= 5) that Ec= 184.482 kJ/mol. The determinate Avrami parameter is around 1.7 which allows suggesting the mechanism is surface crystallization. The crystallization process of the prepared glasses is carried out by heating samples at 550°c for 4 hours and 12 hours. The crystallized phases are identified by XRD. The results of X−ray diffraction analysis confirm that TiO2 acts mainly as network forming units. The crystalline phases Li2WO4 (JCPDS# 01−072−0086) and (JCPDS# 01−087−0409) are formed during the crystallization process. The formation of these crystalline phases into the glasses depends on the time of heating at fixed crystallization temperature. FTIR spectra of the glass−ceramics show nearly the same IR vibrational modes as their parent glasses.

1. Introduction

Glasses and glass-ceramics based phosphates have attracted the attention of many researchers. This is due to their potential applications in technology, like solid electrolyte [1]. All-solid-state batteries using solid electrolytes are expected to have long battery life [2]. Generally, chemical side reactions are inhibited in inorganic solid electrolytes as the lithium ions move through these typical electrolytes. As a result of this, all-solid-state batteries are potentially safer than conventional lithium-ion batteries [3]. Also, they are considered to be ideal batteries for electric vehicles and plug-in hybrid electric vehicles [4]. The solid electrolytes with lithium-ion conductivity are potentially investigated considering their use in power sources [5-6]. Solid electrolytes based phosphate materials are good candidates owing to their easy preparation, low melting point, wide glass-forming region, and simple composition [7-8]. Consequently, in the last decades, scientists paid considerable attention to Li^+ ion glassy electrolytes [9-10].

As well known, the ionic glasses have a wide thermal stability window, but they tend to crystallize at certain temperatures (Tc). For this reason, their direct uses affect the performance of the ionic devices during high-temperature applications [11, 12]. The glass-ceramics derived from glasses present lower conductivity than the parent glasses. This depends on the low ionic conductivity of the precipitated crystallites. Nevertheless, other glass-ceramics exhibit higher conductivity than the pristine glasses of the same compositions, for example, in Ag^+ ion-conducting $AgI–Ag_2O–MoO_3$ glasses. Also, glass-ceramics obtained from the glass $Li_2O–Al_2O_3–TiO_2–P_2O_5$ system exhibited higher conductivity than the host glass matrix. Indeed, the high conductivity is attributed to the formation of the $LiTi_2(PO_4)_3$ phase during crystallization [13]. There are many attempts to optimize ionic conductivity by stabilization the superionic α-phase of ionic compounds in the glass matrix. The first successful attempt has been realized with the stabilization of α-AgI within the glass $AgI–Ag_2O–B_2O_3$ system by rapid quenching. Exceptionally, at room

temperature α-AgI has been established in glass-ceramics of the $AgI–Ag_2O–B_2O_3$ system, which resulted in high Ag^+ ion conductivity of 10^{-1} Ω^{-1} cm^{-1} [14].

Solid electrolytes based on crystalline phosphate materials are widely investigated in all-solid-state batteries, for example, $Li_4P_2O_7$. The XRD data analysis showed that $Li_4P_2O_7$ crystallized in triclinic structure with space group P-1. The linking LiO_4 with P_2O_7 groups allows the formation of a framework with large voids [15]. In this framework, Li^+ ions move easily, thus high conductivity is obtained. In the literature, it reported that $Li_4P_2O_7$ has rather high conductivity (~10^{-1} s/m at 925k) [16]. E. Kartini et al. studied $Li_4P_2O_7$ in the $Li4P_2O_7$-Li_3PO_4 composite with the highest content of 93.56% $Li_4P_2O_7$. This composite achieved high ionic conductivity of 3.85 10^{-5} s/m at room temperature. This ionic conductivity is higher in comparison to the single phase of $LiPO_3$, Li_3PO_4, and $Li_4P_2O_7$. As a result of this, the composite $Li_4P_2O_7$-Li_3PO_4 is a good solid electrolyte for all-solid-state batteries [17].

Another example, Li_2WO_4 compound crystallized in the monoclinic structure with space group (P2/m) and the lattice parameters: a= 9.753A, b= 5.954A, c= 4.994A, α=γ=90° and β= 96.81°. A structural study showed that the presence of some porosity is observed [18]. The presence of porosity is very important for Li^+ ions to move into the $LiWO_4$ structure. The electrical conductivity was carried out in the [200°C-500°C] temperature range. The electrical measurements showed the Li^+ ion conductivity is about 2.18×10^{-7} s/cm at 300°C, and the activation energy is 0.94 eV [19]. The Li_2WO_4 and $Li_4P_2O_7$ ionic conductors have also been reported to exhibit electrical conductivity. Nevertheless, according to our best knowledge, there is no work dealing with the Li_2WO_4-$Li_4P_2O_7$ compound. Our attempts focused on precipitating Li_2WO_4 and $Li_4P_2O_7$ crystallites in Li_2O-Li_2WO_4-TiO_2-P_2O_5 glasses [20, 21]. The precipitation of these crystallites would greatly enhance the ionic conductivity of glass-ceramics. This study is performed to stabilize single or more crystalline phases already known for their high ionic conductivity.

In the present article, we focused on investigating the prepared glasses within the Li_2O-Li_2WO_4-TiO_2-P_2O_5 system. Their characterization was carried out by Raman spectroscopy and chemical durability tests. The crystallization kinetic study is performed by using thermal analysis. The glass-ceramics are characterized by X-ray diffraction and Infrared spectroscopy (IR).

2. Experimental Procedure

2.1. Samples preparation

The phosphate glasses of the $20Li_2O$-$(50-x)Li_2WO_4$-$xTiO_2$-$30P_2O_5$ system (x= 0, 5, 8, 10, and 15 mol %) were prepared according to the protocol described in our previous work [20]. The amorphous state of these colorless glasses is verified by XRD and confirmed by Raman spectroscopic analysis. Glass samples were subjected to controlled thermal heat treatment through a two-step regime. The glasses were first heat-treated at a rate of 10°C/minute to reach 550°C and kept at this temperature for 4 hours. In the second heat-treatment step, the furnace temperature was raised to reach 550°C and kept at this

temperature for 12 hours, sufficient to provide sufficient nucleation sites. The electrical furnace with the samples inside was switched off and then left to cool to room temperature at a rate of 1°C/min. These specific temperatures were collected from DSC measurements. The obtained glass-ceramics were analyzed by a X-ray diffractometer D5000 in the range of $2\theta$from10^{o}to80^{o}. The X-ray data were analyzed by X'Pert High Score Plus software to identify the crystalline phases.

2.2. Raman spectroscopy

The structural properties of the prepared glasses were studied by Raman spectroscopy. The Raman data are obtained at room temperature by using a Horiba Jobin Yvon Lab Ram HR spectrometer. The spectra were measured in backscattering geometry, under excitation with He–Ne laser radiation (632.8 nm) at a power of 12 mW. The exposure time was 3 s, the accumulated number was 10, and the spectral slit width was 1 mm.

2.3. Durability testing

Chemical durability test of the glasses is carried out to determine the dissolution rate in distilled water at 25°C. The prepared blocks of the glasses were placed into a bottle full of distilled water with pH= 6.8. The bottles are suspended in a thermostated bath kept at 30˚C for 250 hours. The dissolution rate, DR, is calculated from the equation DR=Dx/(S.t), where Dx is the mass loss (g), S is the glass surface (cm^2) before the dissolution test, and ‘t’ is time of immersion (min). The pH value of leaching for each glass is measured every 24 hours by a pH-meter.

2.4. Crystallization kinetics

The crystallization kinetics of the glasses is studied by differential scanning calorimetry (DSC). The fine grain powdered sample (< 50 μm) of about 40 mg was placed in an aluminum crucible and heated at a rate of 5°C/min, 8°C/min, 10°C/min, and 12°C/min using a DSC 131 Evo analyzer, from ambient temperature to 550°C. The obtained data are investigated to determine the peak crystallization temperature (T_p).

2.5. Infrared spectroscopy

The structural units formed the glass-ceramics were analyzed by a Fourier Transform Infrared (FTIR) spectrometer. The IR spectra were recorded at room temperature in the frequency range (400–1500) cm^{-1}. The samples were ground to a fine powder and then mixed with KBr powder to prepare pellets for this study.

3. Results And Discussion

3.1. Raman spectroscopy

Figure 1 presents the Raman spectra of the phosphate $20Li_2O$-$(50-x)Li_2WO_4$-$xTiO_2$-$30P_2O_5$ glasses recorded in the wavenumber region 1200 cm^{-1}-150cm^{-1}. The band positions and their assignments are gathered in Table 1. The Raman spectra show different bands situated at different positions: 1055 cm^{-1}, 930 cm^{-1}, 870 cm^{-1}, 740 cm^{-1}, 635-510 cm^{-1}, 372 cm^{-1} and 250 cm^{-1}. The assignments of these bands were made by comparing with literature data [22-25]. From the band positions, we divided the Raman spectra into the three wavenumber regions:

i. In the high wavenumber region, there is a band of low intensity at the position 1055 cm^{-1}. This band is attributed to the asymmetric vibration $V_{as}(P\text{-}O^-)$, Q^1 units. The band at 930 cm^{-1} of high intensity is assigned to the asymmetric vibration of the bond $P\text{-}O^-$ into Q^0 units or to the symmetric vibration $M\text{-}O^-$ in a polyhedron with (M= W, Mo).
ii. For the intermediate region, a band the low intensity at 870 cm^{-1} it observed, associated with the symmetric vibration mode of the bond W–O bond of the WO_6 polyhedron and/or W-O-P bond. Also, a band of low intensity is situated at the position 740 cm^{-1} attributed to the symmetric vibration of the P–O–P bond of the Q^1
iii. In the low wavenumber region, the bands situated between 635 cm^{-1} and 250 cm^{-1} could be attributed to the stretching mode of the $[PO_4]$ units.

After the substitution by TiO_2 in the glass composition (x= 5), two supplementary bands are observed. These bands are situated around the positions 914 cm^{-1} and 742 cm^{-1} attributed to the TiO_4 and TiO_6, respectively [26]. At TiO_2 content increased, Raman spectra change, especially in the region of low frequencies.

This shows that several structural units are present in the various networks. Besides, there is a considerable change in the intensity of the structural units of TiO_4. Such variations suggest that titanium ions occupy distorted octahedral positions and modify the vitreous matrix increasing the number of non-bridging oxygens (NBO). When TiO_2 is present in larger quantities (x> 8), the P=O bond can be broken by structural units of TiO_4, which can cause the creation of new non-bridging oxygen ions facilitating the formation of structural units $[TiO_{6/2}]^{2-}$ [27]. The analysis of Raman spectra shows that the degree of depolymerization of the glass lattice and the quality of TiO_6 structural units increases with increasing TiO_2 content.

3.2. Chemical durability

3.2.1 Weight loss

Chemical durability is expressed by the resistance of the glasses to the attack of chemical species found in a solution. This attack takes place through the process of ion exchange in the hydrated layer. When the

chains are completely surrounded by water, they can separate from the partially hydrated chains and dissolve in solution. Once the hydrated layer is constant, the dissolution is linear over time [28].

Figure 2 represents the evolution of the weight loss at the initial surface ($g.cm^{-2}$) of the glass as a function of time (h). From figure 2, it is noted that the glasses present similar dissolution behavior. We can clearly differentiate two stages or two phases: i) for t <100h, the dissolution is almost linear. ii) for phase 100h <t <h250h, where the dissolution rate slows down. The substitution of Li_2WO_4 by TiO_2 has an observable effect on the dissolution behavior of the synthesized glasses. The dissolution of the glass (x = 0 mol%) is characterized by an initial dissolution, faster than that of the other glasses. The solubility of the glasses studied depends on the degree of substitution of Li_2WO_4 by TiO_2. Indeed, the introduction of TiO_2 in the glass network leads to improved chemical durability of the network. In our similar study, we reported that incorporating Fe_2O_3 into the vitreous network leads to improved chemical durability, which was explained by the formation of a new bond P-O-Fe in place of P-O-P [29]. By analogy, TiO_2 also leads to the enhancement of the chemical durability of the network by the formation of bonds of the type P-O-Ti. These bonds are identified by Raman spectroscopy. These results agree with the thermal analysis, which showed that the introduction of TiO_2 into the phosphate glass network makes the glass matrix harder.

The correlation between chemical durability and thermal analysis confirms that the introduction of TiO_2 into the glass network leads to the strengthening of the chains constituting the glass matrix of the Li_2O-Li_2WO_4-TiO_2-P_2O_5 systems [30].

3.2.2. pH variation

Figure 3 illustrates the evolution of the pH as a function of the immersion time in distilled water (pH ~ 6.8) at a temperature of 30 ° C. The curves showed two zones: i) before 48 h, there is a sudden decrease in pH curves; ii) after 48 h, the pH value is almost constant. This variation in pH depends on the chemical composition of the glass. We can say that the alkali ions and the phosphate ions constitute the glass surface have been released into the solution. This ion exchange plays a major role which that defines the acid-base character of the solution. In fact, decreasing pH curves can be attributed to the disintegration of the phosphate entities. The variation of pH depends on the formation of phosphoric acid controlled by the entities $H_2PO_4^-$ in water [31-34].

As TiO_2 content increases, it is observed that the pH of the solution becomes smaller than the initial solution. These results indicate that the introduction of TiO_2 into the glass network greatly improves chemical durability.

In terms of this chemical study, it is believed that the corrosion mechanism of glasses occurs in two phases: i) a rapid alteration phase where the thermodynamic imbalance between the glass and the altering solution is great, which creates a sudden decrease in pH; ii) a corrosion slowing phase, which is

associated with the saturation of the altering solution. This leads to the formation of a protective layer against diffusion through the surface of the glass.

3.3. Crystallization kinetics by DSC

The activation energy (E_c) of crystallization was calculated by using the following modified form of Kissinger equation (1), established by Matusita and Saka [35].

$Ln(T^2_p/\beta = E_c/(RT_P) + constant$ (1)

Where βR and T_p are the heating rate, the universal gas constant and the peak temperature, respectively.

From the value of the activation energy (E_c), the Avrami exponent (n) was calculated using Augis–Bennett equation (2) [36]:

$n= (2.5/\Delta T)\times(RT^2_P/E_c)$ (2)

Where ΔT is the full width of the exothermic DSC peak at the half-maximum intensity, and (n) is the Avrami exponent or crystallization index. The Avrami exponent (n) had indicated the nucleation and growth mechanism. According to the Johnson–Mehl–Avrami (JMA) theory, (n) was also related to crystallization pattern, n= 2 means that the surface crystallization dominants the overall crystallization, n= 3 means two-dimensional crystallization, n= 4 means that three-dimensional crystallization for bulk materials [37-39].

Figure 4 plots the DSC curves for the composition glass (x= 5) obtained at different heating rates. The DSC curves present a broad crystallization peak shifted to high temperature with an increase in the heating rate. The obtained crystallization temperature (T_p) for the glass (x = 5 mol %) is listed in Table 2. The plot of $ln(Tp^2/\beta)$ versus $1/T_p$ is shown, a straight line is obtained (see Figure 5), and from its slope, the value of E_c can be determined. The value of E_c obtained is 184.482 kJ/mol. The value calculated for (n) is very close to 1.7, suggesting that surface crystallization is dominant during the crystallization of the glasses [40, 41].

3.4. Crystallization of the prepared glasses

Figures 6 and 7 correspond to the X-ray patterns of glass-ceramics derived from the glasses of the $20Li_2O$-$(50-x)Li_2WO_4$-$xTiO_2$-$30P_2O_5$ system. The X-ray patterns gathered in Figure 6 showed the crystallization of crystalline phases into the compounds (x= 0 and 5) Li_2WO_4 (JCPDS# 01-072-0086) and $Li_4P_2O_7$ (JCPDS# 01-087-0409) during 4 hours. At high TiO_2 content (x = 8, 10 et 15 mol%), no crystalline phase formed. Nevertheless, at increasing the heating duration around 12 hours, it observed that the peak intensity of the crystalline phases Li_2WO_4 (JCPDS# 01-072-0086) and $Li_4P_2O_7$ (JCPDS# 01-087-0409) increased for the same composition (x= 0 et 5). But, in the compositions (x= 8, 10 et 15) there are peaks corresponding to the crystalline phases $Li_4P_2O_7$ (JCPDS# 01-087-0409). It seems that the vitreous

network of glasses contains structural units of the pyrophosphate type. The crystallization times of the glasses for 4 hours and 12 hours, insufficient for the formation of crystallized phases contain the titanium within the pieces of the heat-treated glasses.

3.5. Infrared spectra of the glass-ceramics

Figure 8 shows the IR spectra of the prepared glass-ceramics heated at 550°C for 12h. These spectra contain the same principal bands of the phosphate glasses with sharp differences between the glasses (previous work [20]) and their derived glass-ceramics. Both spectra show several absorption bands localized around 1275, 1120, 1085–1050, 940, 860, 745, 605, 510 and 450cm^{-1}. The assignment of the absorption bands was done according to our previous work [20]. In comparison between the absorption bands, it is observed that the FTIR spectra of the glass-ceramics show nearly the same IR vibrational modes as their parent glasses. The IR spectra of the glass-ceramics reveal a few sharp peaks in the far IR region and the mid-region spectrum. Due to the stretching of main phosphate network groups, it appears lower in the intensity of the vibrational bands. This result confirms that the crystalline phases separated where the X-ray data indicate that the formation of two new crystalline phases (Li_2WO_4 and $Li_4P_2O_7$), which are suggested to be somewhat compacted or limited to two phases.

4. Conclusions

The Raman spectra of the prepared glasses show a conversion of metaphosphate units into pyrophosphate and orthophosphate units during the substitution of Li_2WO_4 by TiO_2. Crystallization kinetics of glasses are reported by DSC, where the activation energy depends on the chemical composition of the glass. The parameter Avrami shows that the crystallization of the glasses takes place according to a surface mechanism. In addition, the formation of the crystalline phases depends on the temperature and heat treatment time. Glass-ceramics obtained from the studied glasses submitted to heating at two different durations were exploited by XRD and FTIR. Whereas the crystallized phases into prepared glasses depend on the composition and the conditions of treatment. FTIR analysis has shown that the absorption bands of both spectra (glasses and glass-ceramics) were presented the same bands with quite different. Also, the results of the IR analysis confirmed the formation of the crystalline phases identified by X-ray diffraction.

Declarations

CRediT authorship contribution statement

H. Es-soufi: Conceptualization, Writing - review & editing. **L. Bih**: Supervision. **Alan R. F. Lima**: Visualization. **A. El Bouari**: Visualization. **B. Manoun**: Investigation. **S. Hussain**: Visualization.

Acknowledgments

The authors are grateful to G. Bánhegyi (Medicontur Medical Engineering Ltd., Herceghalmi út 1, Zsámbék 2072, Hungary) for his comments and valuable suggestions.

Competing Interests

The authors declare no competing interests.

References

[1] Ishiyama, T., Suzuki, S., Nishii, J., Yamashita, T., Kawazoe, H., & Omata, T. (2014). Proton conducting tungsten phosphate glass and its application in intermediate temperature fuel cells. Solid State Ionics, 262, 856-859. https://doi.org/10.1016/j.ssi.2013.10.055

[2] S. Hussain, X. Yang, M. Kashif Aslam, A. Shaheen, M. Sufyan Javed, N. Aslam, B. Aslam, G. Liu, G. Qiao, Robust TiN Nanoparticles Polysulfide Anchor for Li–S Storage and Diffusion Pathways Using First Principle Calculations, Chemical Engineering Journal (2019), doi: https://doi.org/10.1016/j.cej.2019.123595

[3] S. Hussain, M.S. Javed, S. Asim, A. Shaheen, A.J. Khan, Y. Abbas, N. Ullah, A. Iqbal, M. Wang, G. Qiao, S. Yun, Novel gravel-like NiMoO4 nanoparticles on carbon cloth for outstanding supercapacitor applications, Ceramics International (2019), doi: https://doi.org/10.1016/j.ceramint.2019.11.118.

[4] Minami, T., Hayashi, A., and Tatsumisago, M. (2006). Recent progress of glass and glass-ceramics as solid electrolytes for lithium secondary batteries. Solid State Ionics. 177, 2715–2720. https://doi.org/10.1016/j.ssi.2006.07.017

[5] V.I. Voronin, E.a. Sherstobitova, V.a. Blatov, G.S. Shekhtman, J. Solid State Chem. 211 (2014) 170–175. https://doi.org/10.1016/j.jssc.2013.12.015

[6] Kartini, E., Nakamura, M., Arai, M., Inamura, Y., Nakajima, K., Maksum, T., ... & Putra, T. Y. S. P. (2014). Structure and dynamics of solid electrolyte (LiI) 0.3 (LiPO3) 0.7. Solid State Ionics, 262, 833-836.. https://doi.org/10.1016/j.ssi.2013.12.041

[7] Minami, T. (1985). Fast ion conducting glasses. Journal of Non-Crystalline Solids, 73(1-3), 273-284. https://doi.org/10.1016/0022-3093(85)90353-9

[8] Knauth, P. (2009). Inorganic solid Li ion conductors: An overview. Solid State Ionics, 180(14-16), 911-916.. https://doi.org/10.1016/j.ssi.2009.03.022

[9] Tatsumisago, M. (2004). Glassy materials based on Li2S for all-solid-state lithium secondary batteries. Solid State Ionics, 175(1-4), 13-18. https://doi.org/10.1016/j.ssi.2004.09.012

[10] Minami, K., Mizuno, F., Hayashi, A., & Tatsumisago, M. (2007). Lithium ion conductivity of the Li2S–P2S5 glass-based electrolytes prepared by the melt quenching method. Solid State Ionics, 178(11-12), 837-841.. https://doi.org/10.1016/j.ssi.2007.03.001

[11] Robertson, A. D., West, A. R., & Ritchie, A. G. (1997). Review of crystalline lithium-ion conductors suitable for high temperature battery applications. Solid State Ionics, 104(1-2), 1-11. https://doi.org/10.1016/S0167-2738(97)00429-3

[12] Henriksen, G. L., & Vissers, D. R. (1994). Lithium-aluminum/iron sulfide batteries. Journal of power sources, 51(1-2), 115-128. https://doi.org/10.1016/0378-7753(94)01965-7

[13] Soman, S., Iwai, Y., Kawamura, J., & Kulkarni, A. (2012). Crystalline phase content and ionic conductivity correlation in LATP glass–ceramic. Journal of Solid State Electrochemistry, 16(5), 1761-1766. https://doi.org/10.1007/s10008-011-1592-4

[14] Tatsumisago, M., Shinkuma, Y., & Minami, T. (1991). Stabilization of superionic α-AgI at room temperature in a glass matrix. Nature, 354(6350), 217-218.

[15] Voronin, V. I., Sherstobitova, E. A., Blatov, V. A., & Shekhtman, G. S. (2014). Lithium-cation conductivity and crystal structure of lithium diphosphate. Journal of Solid State Chemistry, 211, 170-175. https://doi.org/10.1016/j.jssc.2013.12.015

[16] Kartini, E., Yapriadi, V., Jodi, H., Manawan, M., & Panghegar, C. (2020). Solid electrolyte composite Li4P2O7–Li3PO4 for lithium ion battery. Progress in Natural Science: Materials International. https://doi.org/10.1016/j.pnsc.2020.01.020

[17] Horiuchi, H., Morimoto, N., & Yamaoka, S. (1980). The crystal structure of Li2WO4 (IV) and its relation to the wolframite-type structure. Journal of Solid State Chemistry, 33(1), 115-119. https://doi.org/10.1016/0022-4596(80)90554-X

[18] Krishantha, D. M. M., Rajapakse, R. M. G., Tennakoon, D. T. B., & Dias, H. V. R. (2006). Polypyrrole-montmorillonite nanocomposite: a composite fast ion conductor. Journal of composite materials, 40(11), 1009-1021. https://doi.org/10.1177/0021998305056388

[19] Es-soufi, H., Bih, L., Manoun, B., & Lazor, P. (2017). Structure, thermal analysis and optical properties of lithium tungsten-titanophosphate glasses. Journal of Non-Crystalline Solids, 463, 12-18. https://doi.org/10.1016/j.jnoncrysol.2017.02.013

[20]. H. Es-Soufi, L. Bih, B. Manoun & P. Lazor, Structure, thermal analysis and optical properties of lithium tungsten-titanophosphate glasses, (2017). J. Non-Crystalline Solids, 463, 12-18. ttps://doi.org/10.1016/j.jnoncrysol.2017.02.013

[21] Ismail, S. F., Sahar, M. R., & Ghoshal, S. K. (2016). Effects of titanium nanoparticles on self-cleaning and structural features of zinc-magnesium-phosphate glass. *Materials Research Bulletin*, *74*, 502-506.

https://doi.org/10.1016/j.materresbull.2015.11.022

[22] Rao, K. S., Reddy, M. S., Kumar, V. R., & Veeraiah, N. (2008). Dielectric, magnetic and spectroscopic properties of Li2O–WO3–P2O5 glass system with Ag2O as additive. Materials Chemistry and Physics, 111(2-3), 283-292. https://doi.org/10.1016/j.matchemphys.2008.04.012

[23] Marasinghe, G. K., Karabulut, M., Ray, C. S., Day, D. E., Allen, P. G., Bucher, J. J., ... & Shastri, S. (2003). Effects of nuclear waste components on redox equilibria, structural features, and crystallization characteristics of iron phosphate glasses. Ceram. Trans., 93.

[24] Fang, X., Ray, C. S., Moguš-Milanković, A., & Day, D. E. (2001). Iron redox equilibrium, structure and properties of iron phosphate glasses. Journal of non-crystalline solids, 283(1-3), 162-172. https://doi.org/10.1016/S0022-3093(01)00416-1

[25] Krishna, G. M., Kumari, B. A., Reddy, M. S., & Veeraiah, N. (2007). Characterization and physical properties of $Li_2O–CaF_2–P_2O_5$ glass ceramics with Cr_2O_3 as a nucleating agent—Physical properties. Journal of Solid State Chemistry, 180(10), 2747-2755. https://doi.org/10.1016/j.jssc.2007.07.025

[26] Nagarjuna, M., Satyanarayana, T., Gandhi, Y., & Veeraiah, N. (2009). Influence of Ag2O on some physical properties of LiF–TiO2–P2O5 glass system. Journal of alloys and compounds, 479(1-2), 549-556. https://doi.org/10.1016/j.jallcom.2008.12.132

[27] Delahaye-Carrière, F. (1997). Influence de la solution altérante sur la dissolution des verres du système (50-x) Na2O-xCaO-50P2O5 (Doctoral dissertation, Compiègne).

[28] Es-Soufi, H., Bih, L., & Benzineb, M. (2019). Study of Tungsten Phosphate Glasses Containing Fe2O3. New Journal of Glass and Ceramics, 9(3), 33-49. https://doi.org/10.4236/njgc.2019.93004

[29] El Hadrami, A., Mesnaoui, M., Maazaz, M., & Videau, J. J. (2003). Kinetic dissolution of phosphate glasses containing toxic heavy metals. Journal of non-crystalline solids, 331(1-3), 228-239. https://doi.org/10.1016/j.jnoncrysol.2003.08.066

[30] Ma, L., Brow, R. K., & Schlesinger, M. E. (2017). Dissolution behavior of Na2O–FeO–Fe2O3–P2O5 glasses. Journal of Non-Crystalline Solids, 463, 90-101. https://doi.org/10.1016/j.jnoncrysol.2017.02.022

[31] Li, X., Xiao, Z., Luo, M., Dong, X., Du, T., & Wang, Y. (2017). Low melting glasses in ZnO-Fe2O3-P2O5 system with high chemical durability and thermal stability for sealing or waste immobilization. Journal of Non-Crystalline Solids, 469, 62-69. https://doi.org/10.1016/j.jnoncrysol.2017.04.023

[32] Ma, L., Brow, R. K., Ghussn, L., & Schlesinger, M. E. (2015). Thermal stability of Na2O–FeO–Fe2O3–P2O5 glasses. Journal of Non-Crystalline Solids, 409, 131-138.

https://doi.org/10.1016/j.jnoncrysol.2014.11.019

[33] Poluektov, P. P., Schmidt, O. V., Kascheev, V. A., & Ojovan, M. I. (2017). Modelling aqueous corrosion of nuclear waste phosphate glass. Journal of Nuclear Materials, 484, 357-366. https://doi.org/10.1016/j.jnucmat.2016.10.033

[34] Kissinger, H. E. (1956). Variation of Pedk Temperature With Hedting Rote in Differentidl Thermal Andlysis. Journal of research of the National Bureau of Standards, 57, 217.

[35] Augis, J. A., & Bennett, J. E. (1978). Calculation of the Avrami parameters for heterogeneous solid state reactions using a modification of the Kissinger method. Journal of thermal analysis, 13(2), 283-292. https://doi.org/10.1007/BF01912301

[36] Avrami, M. (1939). Kinetics of phase change. I General theory. The Journal of chemical physics, 7(12), 1103-1112. https://doi.org/10.1063/1.1750380

[37] Avrami, M. (1940). Kinetics of phase change. II transformation-time relations for random distribution of nuclei. The Journal of chemical physics, 8(2), 212-224. https://doi.org/10.1063/1.1750631

[38] Avrami, M. (1941). Kinetics of phase change. III: Granulation, phase change and microstructure. Journal of chemical physics, 9, 177-184. https://doi.org/10.1063/1.1750872

[39] Tosić, M. B., Dimitrijević, R. Ž., & Mitrović, M. M. (2003). The crystallization of calcium phosphate glass with the ratio [CaO]/[P 2 O 5]< 1. Journal of materials science, 38(9), 1983-1994. https://doi.org/10.1023/A:1023585321475

[40] Haily, E., Bih, L., El Bouari, A., Lahmar, A., El Marssi, M., & Manoun, B. (2020). Structural, optical, and dielectric properties of Bi2O3-K2O-TiO2-P2O5 glasses and related glass-ceramics. Phase Transitions, 1-18. https://doi.org/10.1080/01411594.2020.1837369

[41] ElBatal, F. H., Marzouk, M. A., & ElBatal, H. A. (2016). Optical and crystallization studies of titanium dioxide doped sodium and potassium silicate glasses. Journal of Molecular Structure, 1121, 54-59. https://doi.org/10.1016/j.molstruc.2016.05.052

Tables

Table 1. Raman band assignments in the 1200-100 cm^{-1} range frequency for the studied phosphate glasses.

Position of band (cm^{-1})	Band assignment
1055	$v_s(PO_2)^-$,Q^2
930	v_{as}(P-O-P)/V_{as}(P-O-M) (M= Mo. Ti)
870	O-Mo-O/MO_4/MO_6(M= Mo. Ti)
740	v_s(P-O-P), Q^1
635-510	v_s(P-O-P), Q^2
372	V_s(M-O-M)(M= Mo, Ti)
250	δ(PO_4)

Table 2: Crystallization temperature of the glass (x = 5 mol %) at different heat crystallization rates.

Glass	β(°C/min^{-1})	T_p	ΔT	Avrami parameter (n)
x= 5	5	524	14	2.20
	8	528	16	1.96
	10	532	22	1.45
	12	534	25	1.28

Figures

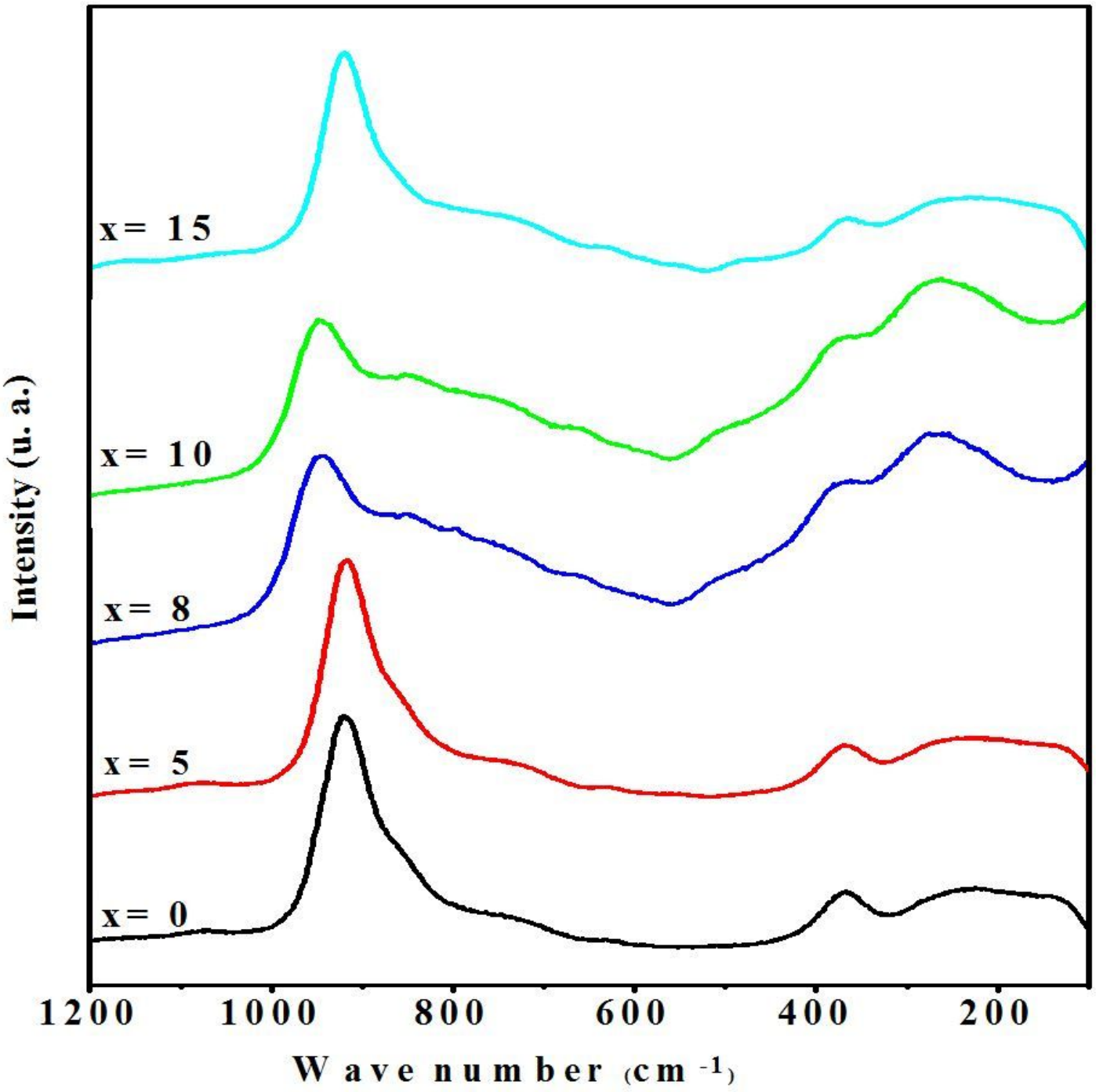

Figure 1

Raman spectra of the studied glasses

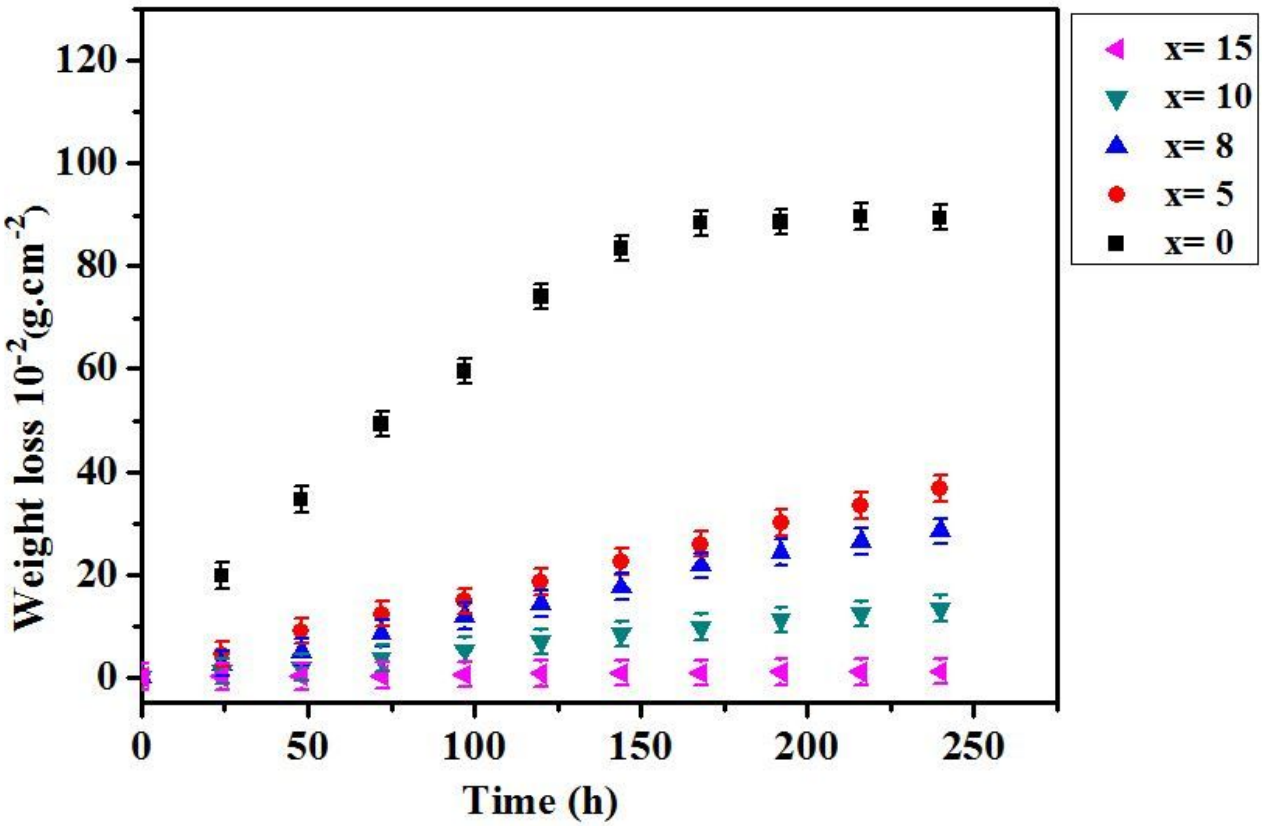

Figure 2

Evolution of the weight loss of the glasses as a function of time (h)

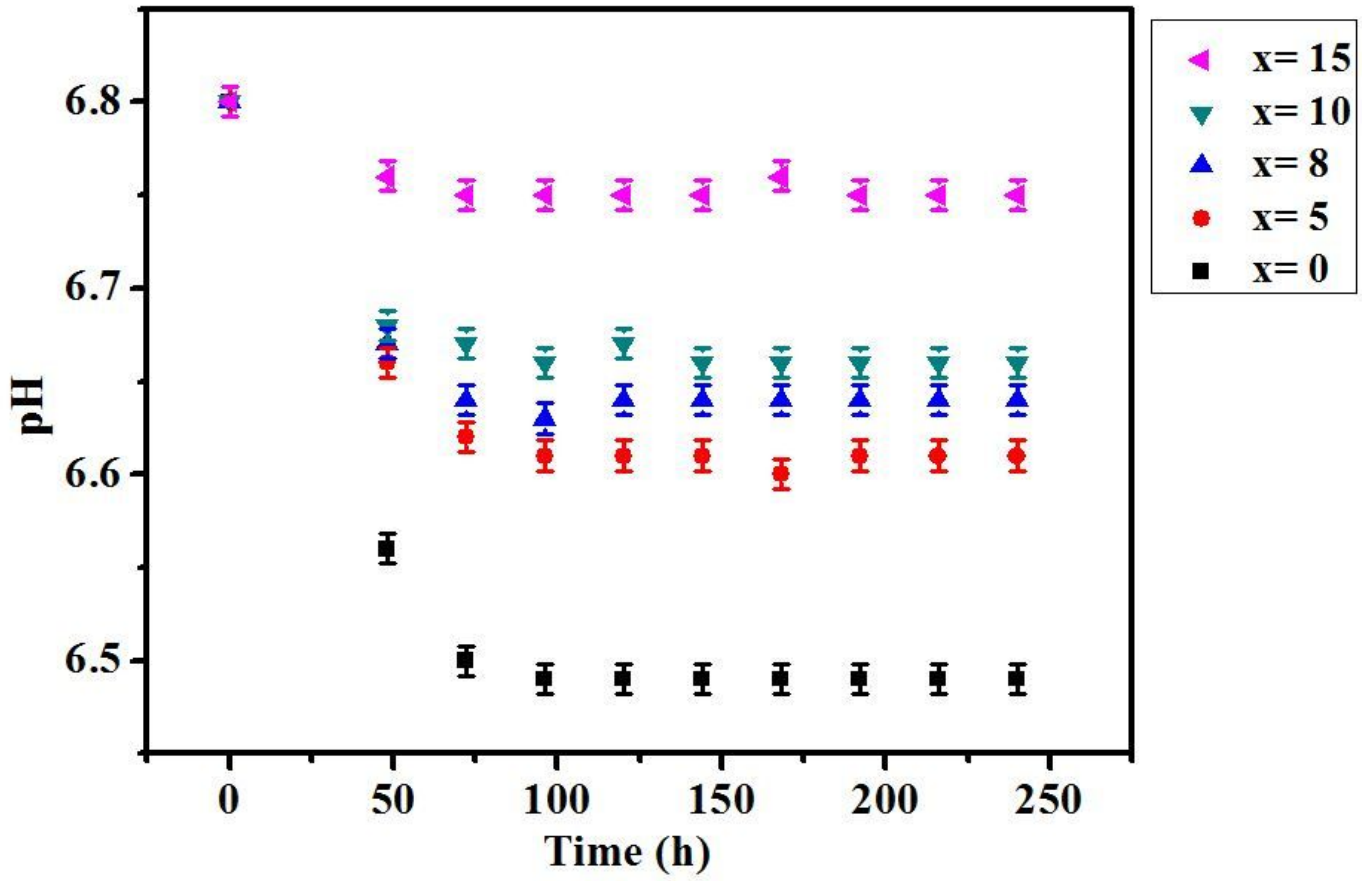

Figure 3

Evolution of the pH of the glasses as a function of time (h)

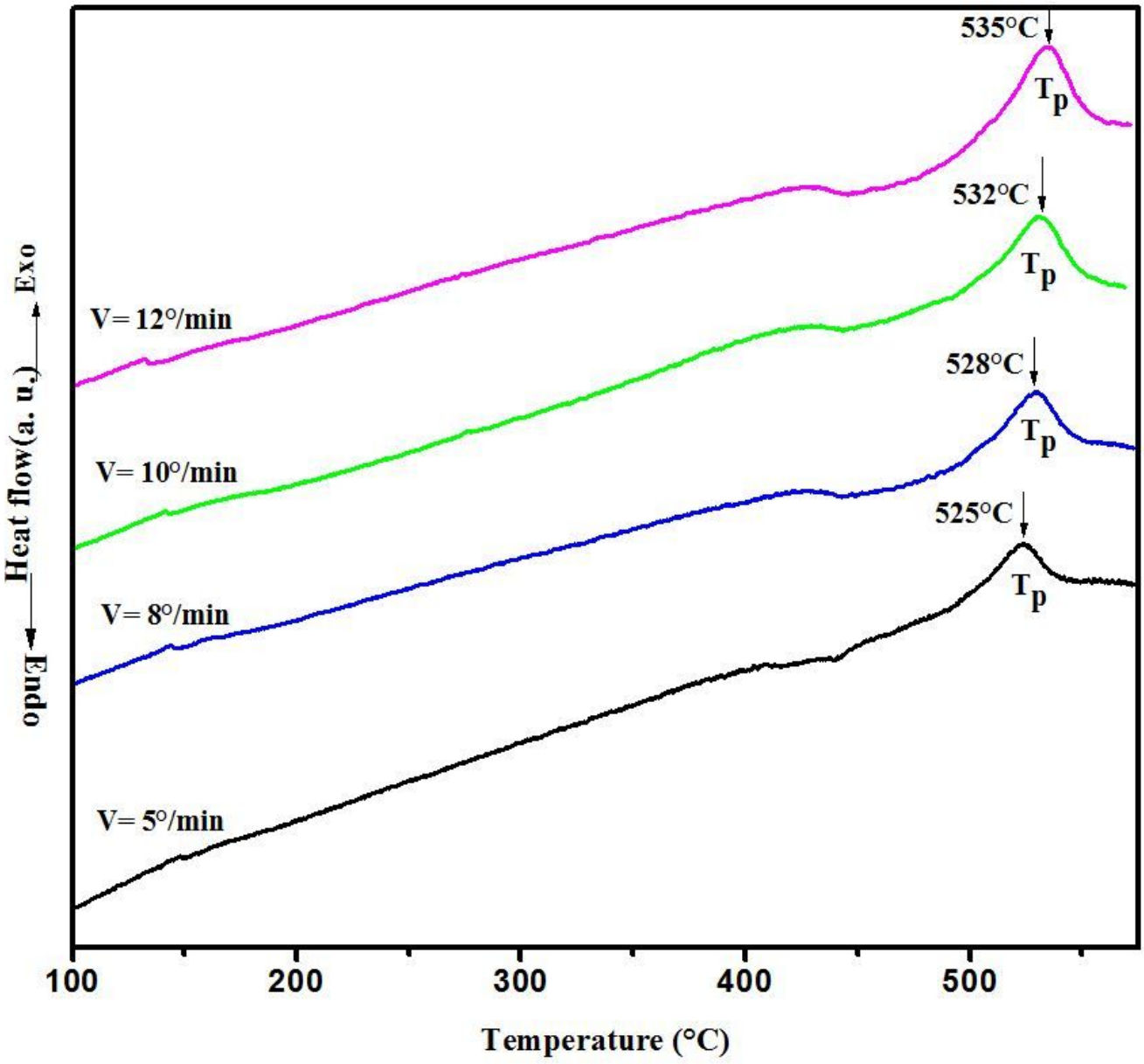

Figure 4

DSC curves for the glass (x = 5) under different heating rates

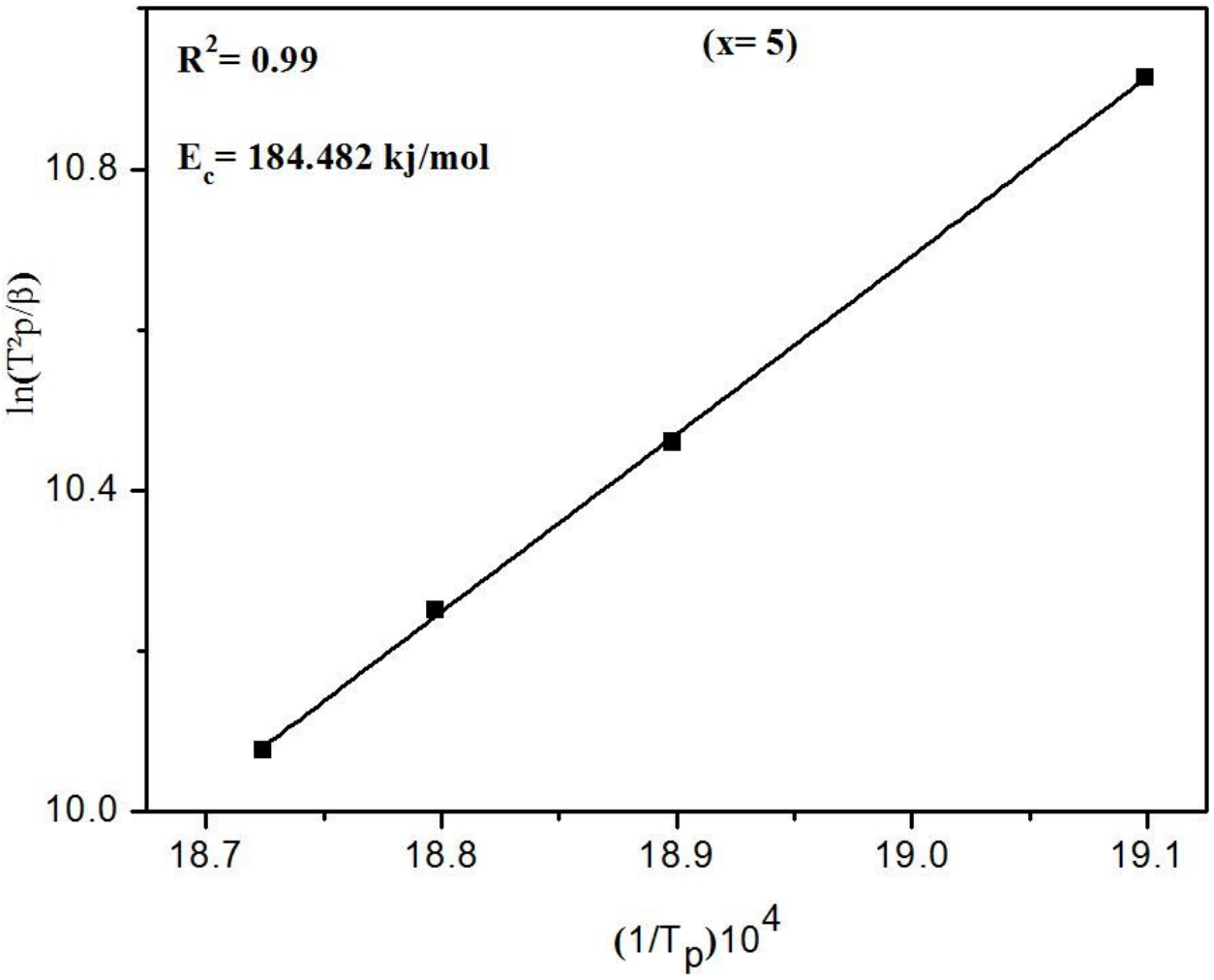

Figure 5

Plot of ln(T2π/β) versus inverse temperature for the glass

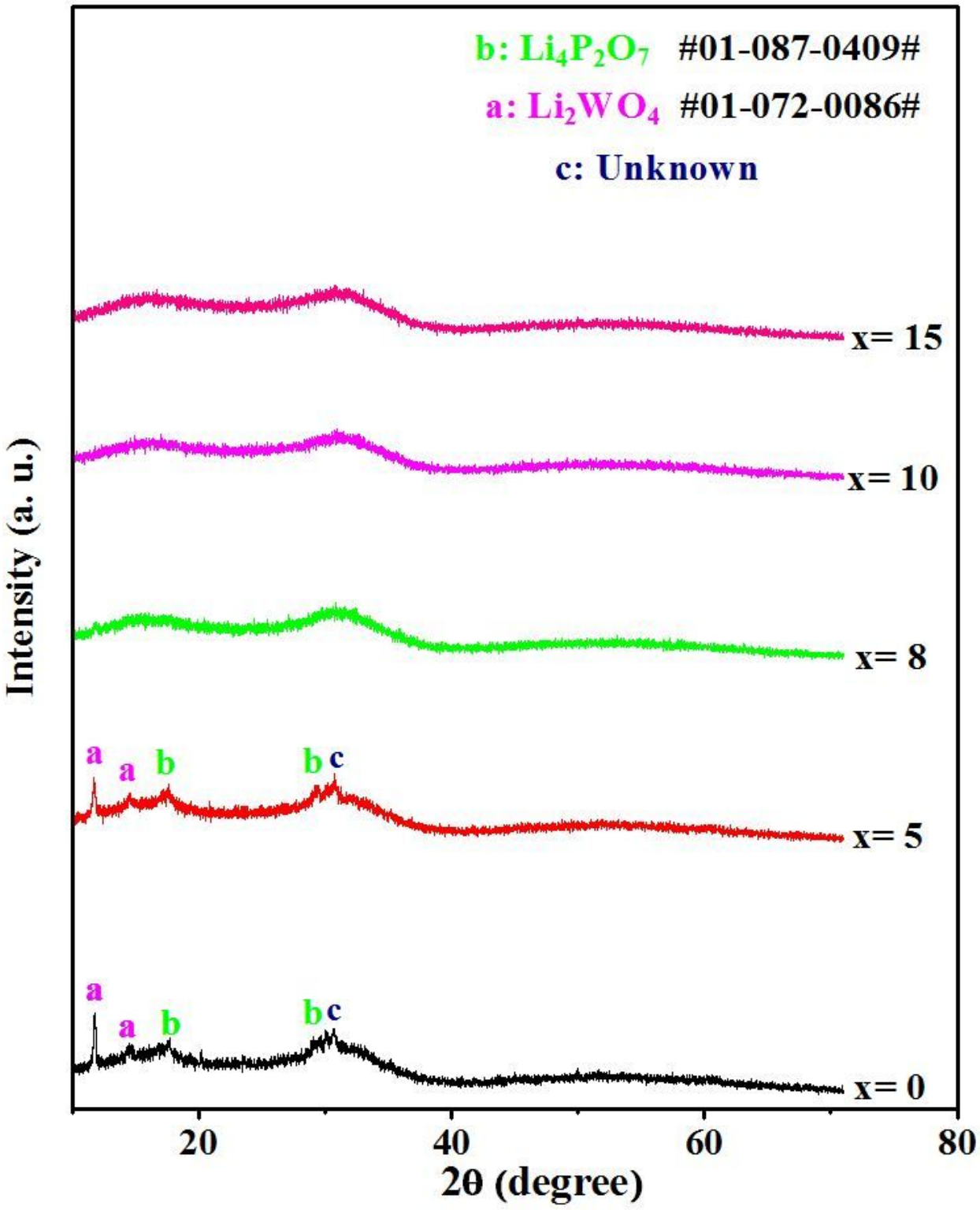

Figure 6

XRD patterns of the crystallized glasses at 550°C for 4 h

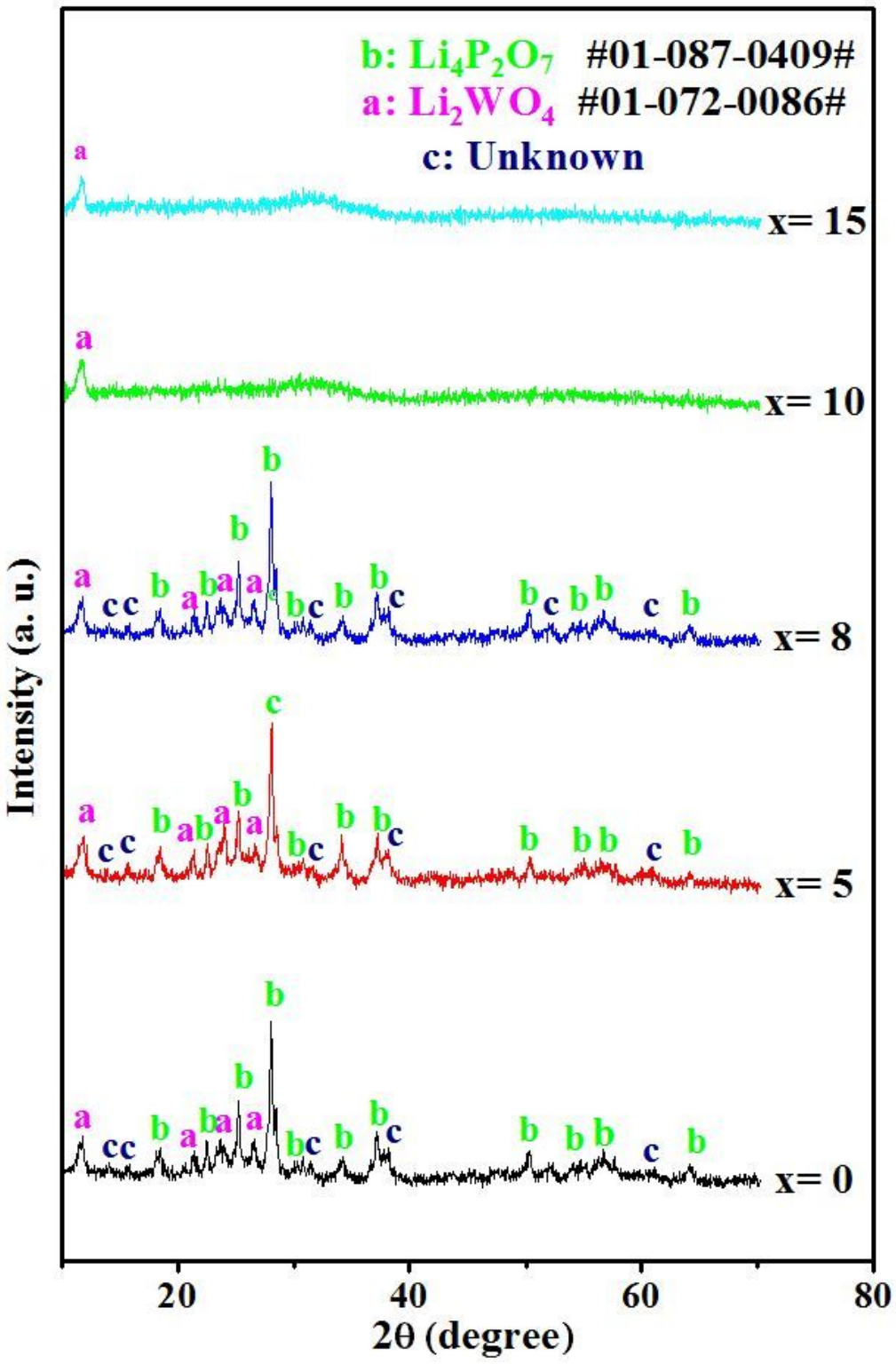

Figure 7

XRD patterns of the crystallized glasses at 550°C for 12 h

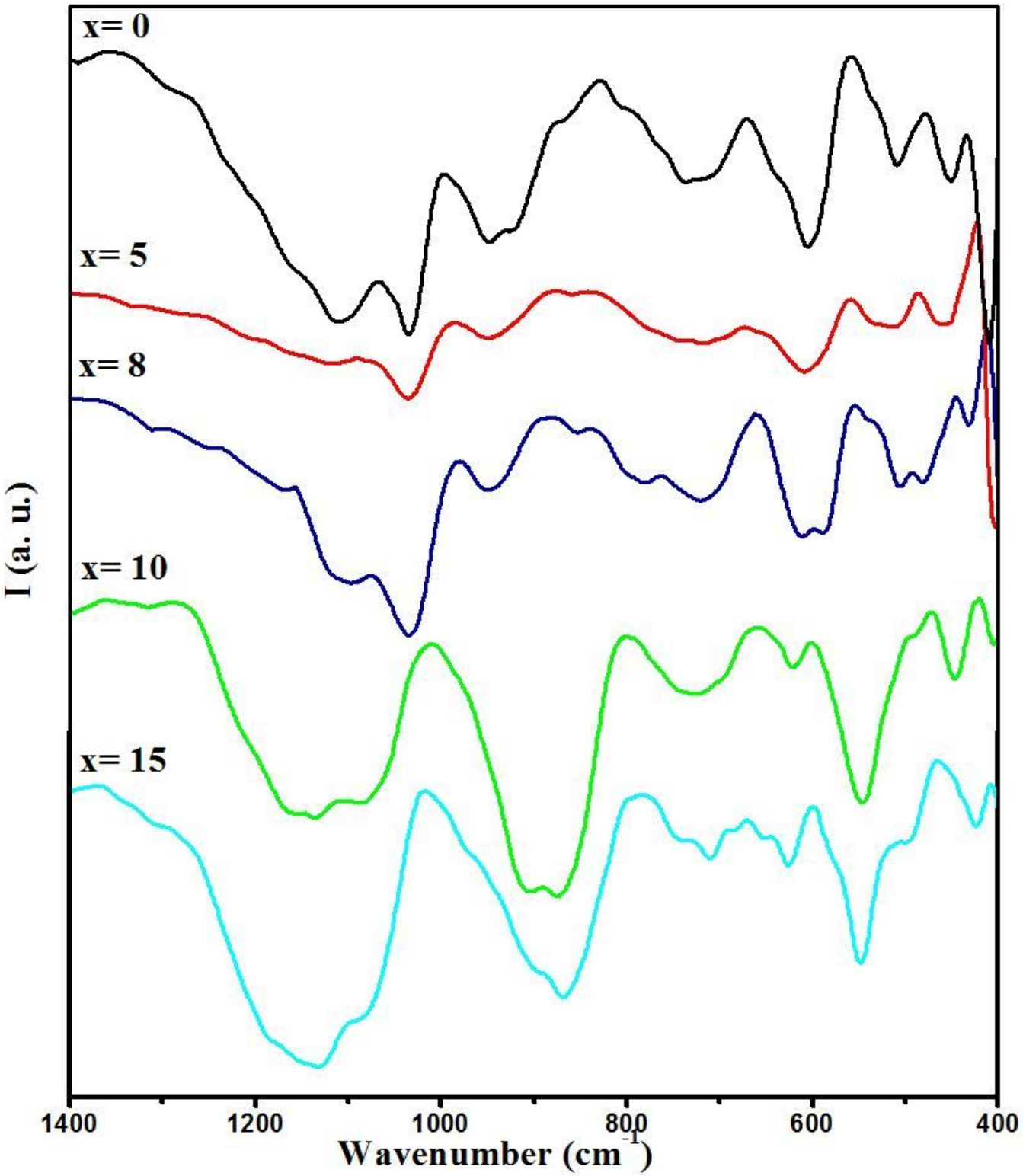

Figure 8

FTIR spectra of the crystallized glasses at 550°C for 12h